Synthetic Metals 162 (2012) 2294–2301

Contents lists available at SciVerse ScienceDirect

Synthetic Metals

journal homepage: www.elsevier.com/locate/synmet

White polymer light-emitting diode materials with efficient electron injection backbone containing polyfluorene, oxadiazole and quinoxaline derivatives

Myung Hee Han[a], Ho Jun Song[a], Tae Ho Lee[a], Jang Yong Lee[b], Doo Kyung Moon[a,*], Jung Rim Haw[a,*]

[a] Department of Materials Chemistry and Engineering, Konkuk University, 1 Hwayang-dong, Gwangjin-gu, Seoul 143-701, Republic of Korea
[b] Energy Materials Research Center, Korea Research Institute of Chemical Technology, P.O. Box 107, Yuseong, Daejeon 305-600, Republic of Korea

ARTICLE INFO

Article history:
Received 2 October 2012
Received in revised form 23 October 2012
Accepted 7 November 2012
Available online 12 December 2012

Keywords:
Oxadiazole
Quinoxaline
Conjugated polymer
WPLED

ABSTRACT

Copolymer including dithienylquinoxaline (TQ) (<0.1 mol%) as a dopant and oxadiazole derivative as a side chain has been synthesized on a Polyfluorene (PF) backbone based on the Suzuki coupling reaction. The UV–vis spectra of polymers showed similar behaviors in the solution and on the film. However, PL spectra were similar to that of PF in solution, but the peak around 524 nm increased as the amounts of TQ were increased in the casting film. With increase in TQ, effective Forster energy transfer (from PF and PFOxd15 to TQ) was observed. According to CV measurement, HOMO and LUMO levels declined as the amount of oxadiazole derivative increased. In case of PFOxd15TQ10, the luminous efficiency and power efficiency were 1.23 cd/A and 0.64 lm/W, respectively with a maximum brightness of 6940 cd/m^2. CIE coordinates were close to pure white (0.33, 0.39).

1. Introduction

For the past decades, π-conjugated polymer has been applied to diverse applications such as organic light-emitting diodes (OLEDs) [1–6], organic photovoltaic cells (OPVs) [7–9], organic thin-film transistors (OTFTs) [10–12], and liquid crystal application (LC) [13]. In particular, polymer light-emitting diodes (PLED) present advantages in large-area fabrication methods, such as ink-jet and screen printing with solution processes. As a result, the material has drawn great attention as a next-generation material to replace vacuum deposition with small molecules. Thanks to its convenience and flexibility, polymer film has been popular in the flexible display sector [8,14].

A number of studies have been focusing on PLED materials in various colors since the development of poly(phenylenevinylene) in 1990 [15]. It has been reported that polyfluorene(PF) [16], poly(phenylenevinylene)(PPV) [17], and poly(methoxy, ethylhexyloxy phenylene vinylene)(MEH-PPV) [18] are the representative blue-emitting, green-emitting, and orange & red-emitting materials, respectively. Full-color displays have been enabled by such polymers [4,8].

Recently, there have been more studies on white polymer light-emitting diodes (WPLED) that introduced diverse chromophores to the blue emitting material, PF. If chromophore is introduced to a PF backbone, aggregation and excimers are suppressed. As a result, effective energy transfer occurs in such materials. Therefore, high-efficiency WPLEDs can be realized [19,20]. Recently, we introduced a small amount of low-band-gap chromophore (<0.3 mol%) to a PF backbone and had it copolymerized. Depending on the dopant mol ratio, various color changes (white, green, yellow, etc.) could be detected with high efficiency [5].

The electron-deficient quinoxaline derivative is a leading orange-emitting chromophore. Due to thermal and electrochemical stability and high PL and EL efficiency, the quinoxaline derivative has been widely used in white and orange light-emitting polymers [21–23]. In addition, the quinoxaline derivative can be easily tuned in structure with high solubility. Therefore, electronic characteristics can be changed by introducing various substituents [24,25].

Recently, there have been many studies on the introduction of oxadiazole derivative, which has superior electron withdrawing characteristics to those of the PF backbone [26]. If the oxadiazole derivative is introduced to the PF backbone, electron injection becomes effective with high efficiency [27,28]. However, green emission at 450–500 nm increases due to oxadiazole derivative. If the amount of oxadiazole derivative increases, the external quantum efficiency and charge balance decline due to dominant shield effects [29,30].

In this study, 0.03–0.1 mol% of quinoxaline derivative was adopted as dopant with an orange emitter and PF as a host. For effective electron transfer, the oxadiazole derivative was introduced to the PF backbone as a side chain. The Forster energy

* Corresponding authors. Tel.: +82 2 450 3499; fax: +82 2 2201 6447.
E-mail address: jrhaw@konkuk.ac.kr (J.R. Haw).

0379-6779/$ – see front matter © 2012 Elsevier B.V. All rights reserved.
http://dx.doi.org/10.1016/j.synthmet.2012.11.004

transfer was investigated, as well as the charge trapping and charge balance effects between host and dopant, and the optimum mol concentration for effective white-emitting polymer was realized.

2. Experiment

2.1. Instruments and characterization

Unless otherwise specified, all the reactions were carried out under nitrogen atmosphere. Solvents were dried by standard procedures. Column chromatography was performed with the use of silica gel (230–400 mesh, Merck) as the stationary phase. ^{1}H NMR spectra were performed in a Bruker ARX 400 spectrometer using solutions in $CDCl_3$, and chemical concentrations were recorded in units of ppm with TMS as the internal standard. Electronic absorption spectra were measured in chloroform using a HP Agilent 8453 UV-Vis spectrophotometer. Photoluminescent spectra were recorded by a Perkin Elmer LS 55 luminescence spectrometer. Cyclic voltammetry experiments were performed with a Zahner IM6eX Potentionstat/Galvanostat. All measurements were carried out at room temperature with a conventional three-electrode configuration consisting of platinum working and auxiliary electrodes and a nonaqueous Ag/AgCl reference electrode at the scan rate of 50 mV/s. The solvent in all experiments was acetonitrile and the supporting electrolyte was 0.1 M tetrabutyl ammonium-tetrafluoroborate. TGA measurements were performed on a NETZSCH TG 209 F3 thermogravimetric analyzer. All GPC analyses were made by using THF as the eluant and polystyrene standard as the reference.

2.2. EL device fabrication and characterization

The fabricated device structure was ITO/PEDOT:PSS/polymer/BaF_2/Ba/Al. All of the polymer light-emitting diodes were prepared using the following device fabrication procedure. Glass/indium tin oxide(ITO) substrates [Sanyo, Japan(10 Ω/γ)] were sequentially patterned lithographically, cleaned with detergent, and ultrasonicated in deionized water, acetone and isopropyl alcohol. Then, the substrates were dried on a hotplate at 120 °C for 10 min and treated with oxygen plasma for 10 min in order to improve the contact angle just before the film coating process. Poly(3,4-ethylenedioxythiophene): poly(styrene-sulfonate) (PEDOT:PSS, Baytron P 4083 Bayer AG) was passed through a 0.45-μm filter before being deposited onto ITO at a thickness of ca. 32 nm through spin-coating at 4000 rpm in air, and then dried at 120 °C for 20 min inside a glove box. The light-emitting polymer layer was then deposited onto the film by spin coating a polymer solution in chlorobenzene (1.5 wt.%) at a speed of 1000 rpm for 30 s on top of the PEDOT:PSS layer. The device was thermally annealed at 90 °C for 30 min in a glove box. The device fabrication was completed by depositing thin layers of BaF_2 (1 nm), Ba (2 nm) and Al (200 nm) at pressures less than 10^{-6} Torr. The active area of the device was 9.0 mm^2. Finally, the cell was encapsulated using UV-curing glue (Nagase, Japan). EL spectra, Commission Internationale de l'Eclairage (CIE) coordinates, current–voltage, and brightness–voltage characteristics of devices were measured with a Spectrascan PR670 spectrophotometer in the forward direction, and a computer-controlled Keithley 2400 under ambient conditions.

2.3. Materials & synthesis of monomers

All reagents were purchased from Aldrich, Acros or TCI companies. All chemicals were used without further purification. The following compounds were synthesized following modified literature procedures: 5,8-bis(5-bromothiophen-2-yl)-2,3-bis(4-(hexyloxy)phenyl)quinoxaline **A** [6], 5,5′-(4,4′-(6,6′-(2,7-dibromo-9H-fluorene-9,9-diyl)bis(hexane-6,1-diyl))bis(oxy)bis(4,1-phenylene))bis(2-(4-tert-butylphenyl)-1,3,4-oxadiazole) **B** [9], 2,2′-(9,9-dioctyl-9H-fluorene-2,7-diyl)bis(4,4,5,5-tetramethyl-1,3,2-dioxaborolane) **C** [5].

2.4. Polymerization

Reaction monomers, $(PPh_3)_4Pd(0)$ (1.5 mol%) and Aliquat 336 were dissolved in a mixture of toluene and an aqueous solution of 2 M K_2CO_3. The solution was refluxed for 72 h with vigorous stirring in nitrogen atmosphere, and then excess amounts of bromobenzene, as an end capper, was added and stirring continued for 12 h. The whole mixture was poured into methanol. The precipitate was filtered off, and purified with methanol, acetone, hexane, chloroform in soxhlet.

PFOxd05. 9,9-Dioctylfluorene-2,7-dibromofluorene (0.45 equiv.), 2,2′-(9,9-dioctyl-9H-fluorene-2,7-diyl)bis(4,4,5,5-tetramethyl-1,3,2-dioxaborolane) **(C)** (0.50 equiv.), 5,5′-(4,4′-(6,6′-(2,7-dibromo-9H-fluorene-9,9-diyl)bis(hexane-6,1-diyl))bis(oxy)bis (4,1-phenylene))bis(2-(4-tert-butylphenyl)-1,3,4-oxadiazole) **(B)** (0.05equiv); Yield: 0.22 g (51%); ^{1}H NMR (400 MHz; $CDCl_3$; Me_4Si): δ = 7.85–7.83 (m), 7.71–7.25 (m), 3.90 (m), 2.11 (m), 1.25–1.13 (m), 0.83–0.79 (m).

PFOxd15. 9,9-Dioctylfluorene-2,7-dibromofluorene (0.35 equiv.), 2,2′-(9,9-dioctyl-9H-fluorene-2,7-diyl)bis(4,4,5,5-tetramethyl-1,3,2-dioxaborolane) **(C)** (0.50 equiv.), 5,5′-(4,4′-(6,6′-(2,7-dibromo-9H-fluorene-9,9-diyl)bis(hexane-6,1-diyl))bis(oxy)bis (4,1-phenylene))bis(2-(4-tert-butylphenyl)-1,3,4-oxadiazole) **(B)** (0.15 equiv.); Yield: 0.25 g (58%); ^{1}H NMR (400 MHz; $CDCl_3$; Me_4Si): δ = 7.85–7.83 (m), 7.71–7.25 (m), 2.11 (m), 3.90 (m), 1.25–1.13 (m), 0.83–0.79 (m).

PFOxd15TQ03. 9,9-Dioctylfluorene-2,7-dibromofluorene (0.34 equiv.), 2,2′-(9,9-dioctyl-9H-fluorene-2,7-diyl)bis(4,4,5,5-tetramethyl-1,3,2-dioxaborolane) **(C)** (0.50 equiv.), 5,5′-(4,4′-(6,6′-(2,7-dibromo-9H-fluorene-9,9-diyl)bis(hexane-6,1-diyl))bis(oxy)bis (4,1-phenylene))bis(2-(4-tert-butylphenyl)-1,3,4-oxadiazole) **(B)** (0.15equiv), 5,8-bis(5-bromothiophen-2-yl)-2,3-bis(4-(hexyloxy) phenyl)quinoxaline **(A)** (0.0003 equiv.); Yield: 0.20 g (46%); ^{1}H NMR (400 MHz; $CDCl_3$; Me_4Si): δ = 7.85–7.83 (m), 7.71–7.25 (m), 3.90 (m), 2.11 (m), 1.25–1.13 (m), 0.83–0.79 (m).

PFOxd15TQ05. 9,9-Dioctylfluorene-2,7-dibromofluorene (0.34 equiv.), 2,2′-(9,9-dioctyl-9H-fluorene-2,7-diyl)bis(4,4,5,5-tetramethyl-1,3,2-dioxaborolane) **(C)** (0.50 equiv.), 5,5′-(4,4′-(6,6′-(2,7-dibromo-9H-fluorene-9,9-diyl)bis(hexane-6,1-diyl))bis(oxy)bis (4,1-phenylene))bis(2-(4-tert-butylphenyl)-1,3,4-oxadiazole) **(B)** (0.15 equiv.), 5,8-bis(5-bromothiophen-2-yl)-2,3-bis(4-(hexyloxy) phenyl)quinoxaline **(A)** (0.0005 equiv.); Yield: 0.21 g (48%); ^{1}H NMR (400 MHz; $CDCl_3$; Me_4Si): δ = 7.85–7.83 (m), 7.71–7.25 (m), 3.90 (m), 2.11 (m), 1.25–1.13 (m), 0.83–0.79 (m).

PFOxd15TQ10. 9,9-Dioctylfluorene-2,7-dibromofluorene (0.34 equiv.), 2,2′-(9,9-dioctyl-9H-fluorene-2,7-diyl)bis(4,4,5,5-tetramethyl-1,3,2-dioxaborolane) **(C)** (0.50 equiv.), 5,5′-(4,4′-(6,6′-(2,7-dibromo-9H-fluorene-9,9-diyl)bis(hexane-6,1-diyl))bis(oxy)bis (4,1-phenylene))bis(2-(4-tert-butylphenyl)-1,3,4-oxadiazole) **(B)** (0.15 equiv.), 5,8-bis(5-bromothiophen-2-yl)-2,3-bis(4-(hexyloxy) phenyl)quinoxaline **(A)** (0.001 equiv.); Yield: 0.21 g (48%); ^{1}H NMR (400 MHz; $CDCl_3$; Me_4Si): δ = 7.85–7.83 (m), 7.71–7.25 (m), 3.90 (m), 2.11 (m), 1.25–1.13 (m), 0.83–0.79 (m).

PFTQ10. 9,9-Dioctylfluorene-2,7-dibromofluorene (0.49 equiv.), 2,2′-(9,9-dioctyl-9H-fluorene-2,7-diyl)bis(4,4,5,5-tetramethyl-1,3,2-dioxaborolane) **(C)** (0.50 equiv.), 5,8-bis(5-bromothiophen-2-yl)-2,3-bis(4-(hexyloxy)phenyl)quinoxaline **(A)** (0.001 equiv.); Yield: 0.19 g (43%); ^{1}H NMR (400 MHz; $CDCl_3$; Me_4Si):

δ = 7.85–7.83 (m), 7.71–7.25 (m), 2.11 (m), 1.25–1.13 (m), 0.83–0.79 (m).

3. Results and discussion

3.1. Synthesis and characterization of the polymers

As shown in Scheme 1, a total of 7 polymers were polymerized through Suzuki coupling reaction by using different mol ratios (monomers a, b and c) with 70–80% yield ratio. The polymerization was reacted at 90 °C for 72 h with palladium catalyst (0) and 2 M potassium carbonate solution. In addition, aliquot 336 and toluene were used as surfactant and solvent, respectively. Once the polymerization was completed, it was end-capped with bromobenzene. All polymers were purified with soxhlet in order of methanol, acetone and chloroform, and the chloroform fraction was recovered. All polymers dissolved in general organic solvents such as THF, chloroform, chlorobenzene and dichlorobenze, and a homogenous and transparent film has been formed through spin-coating (Scheme 2).

In the H NMR spectra obtained (see Fig. S1), an aromatic peak was found at 7.0–8.0 ppm, while a proton peak originating from an aliphatic peak was detected at 0.8–5.0 ppm. A proton peak from the small amount (10^{-4} mol against total monomer) of the dithienylquinoxaline (TQ) dopant was not observed. As shown in the references, the actual dopant ratio could not be measured through NMR, FT-IR or elemental analysis against the dopant ratio 0.5 mol% or below [5,31]. As shown in Table 1, according to the measurement of GPC with polystyrene as the standard, the number average molecular weight of all polymers ranged from 12,500 to 26,000. The degree of polymerization was similar to that of general EL polymer [5]. The polydispersity indices (PDI) showed a very narrow distribution (1.68–2.04).

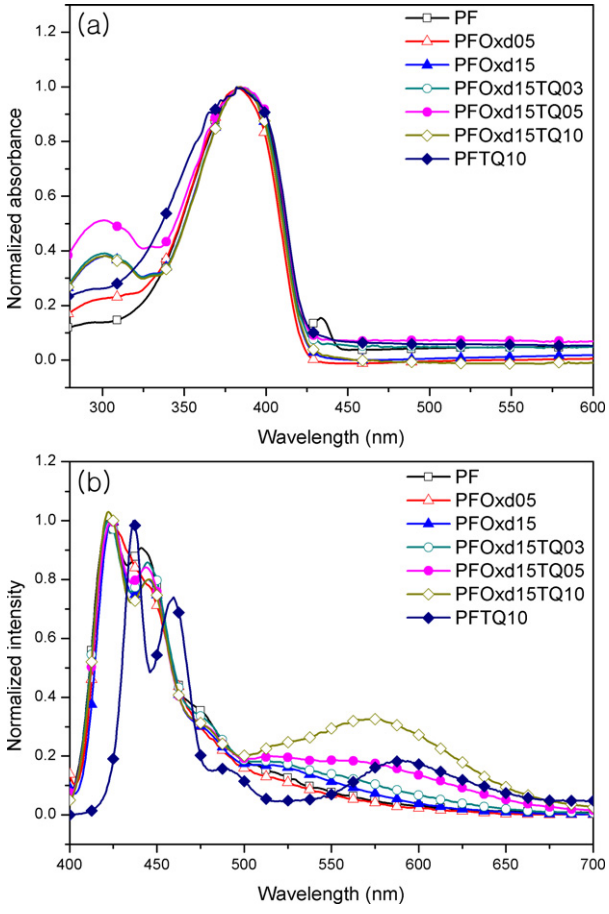

Fig. 1. (a) UV–vis absorption spectra (b) PL emission spectra in thin film of polymers.

Table 1
Physical properties of the polymers.

Polymer	M_n (kg/mol)	M_w (kg/mol)	PDI	T_d[a] (°C)
PF	22.6	41.5	1.83	365
PFOxd05	22.6	41.5	1.83	392
PFOxd15	26.3	45.8	1.74	392
PFOxd15TQ03	23.1	31.2	1.75	402
PFOxd15TQ05	17.5	31.8	1.78	370
PFOxd15TQ10	25.6	40.8	1.68	402
PFTQ10	12.5	25.7	2.04	403

[a] Temperature resulting in 5% weight loss based on initial weight.

Thermal analysis through TGA (see Fig. S2) indicated high thermal stability (around 400°) at 5 wt.% loss, which reveals applicability to display application sectors in which high thermal stability (400 °C or higher) is required [5,32]. In addition, thermal characteristics similar to PF were found in all polymers, which means that the dopant and oxadiazole derivatives introduced to the PF backbone had no effect on polymer rigidity. The weight loss of 45–50% at 400–500 °C is the result of the degradation of the skeletal PF backbone chain structure. The PF backbone is decomposed to oligomers or other short chain structures [33].

3.2. Optical and electrochemical properties

Fig. 1 reveals the UV–visible spectra and PL spectra of all polymer films. As shown in Fig. 1(a), all polymers were characterized by λ_{max} = 382 nm (4–7 nm blue-shifted compared to solution) in terms of maximum absorption peak in UV–visible spectra [28,31]. This kind of result was caused by π–π^* transition distribution between polymer chains in the film formation by fluorene polymer [35]. The absorption peak of the TQ derivative (dopant) was not observed because of the small amount of dopant used.

In case of PL spectra, as shown in Fig. 1(b), as TQ content increased, the 570 nm emission peak broadened, unlike for the solution, because of increases in the intermolecular interaction among the polymer main chains.[19] In addition, the red-shift phenomenon which occurs on the film due to strong intermolecular interaction among polymers significantly declined in the PFOxd series polymer containing the oxadiazole derivative. The PFTQ10, which did not contain oxadiazole derivative, was red-shifted by 20 nm, while PFOxd polymers were red-shifted by 5–7 nm compared to solution because the oxadiazole derivative interrupted the strong π–π stacking by suppressing strong intermolecular interaction among polymers [34]. Therefore, recombination of excited electrons occurs frequently in the polymer backbone upon electron injection due to weak π–π stacking.

According to the comparison between the UV–vis spectrum of TQ and PL spectra of PF and PFOxd15 (see Fig. S4), the absorption spectrum of TQ derivative was overlapped in the PL spectra of PF and PFOxd15, which means effective absorption of PF and PFOxd15 emission energy by TQ. Therefore, effective Forster energy transfer from PF and PFOxd15 backbone to TQ derivative would occur in the copolymer.

Fig. 2 showed the electrochemical properties of the polymers which were measured through cyclic voltammetry (CV). The highest occupied molecular orbital (HOMO) levels of polymers were calculated using the oxidation onset value of polymers and the reference energy level (4.8 eV below the vacuum level) of ferrocene as follows:

$$\text{HONO (eV)} = -4.8 - (E_{\text{onset}} - E_{1/2}(\text{Ferocene})) \quad (1)$$

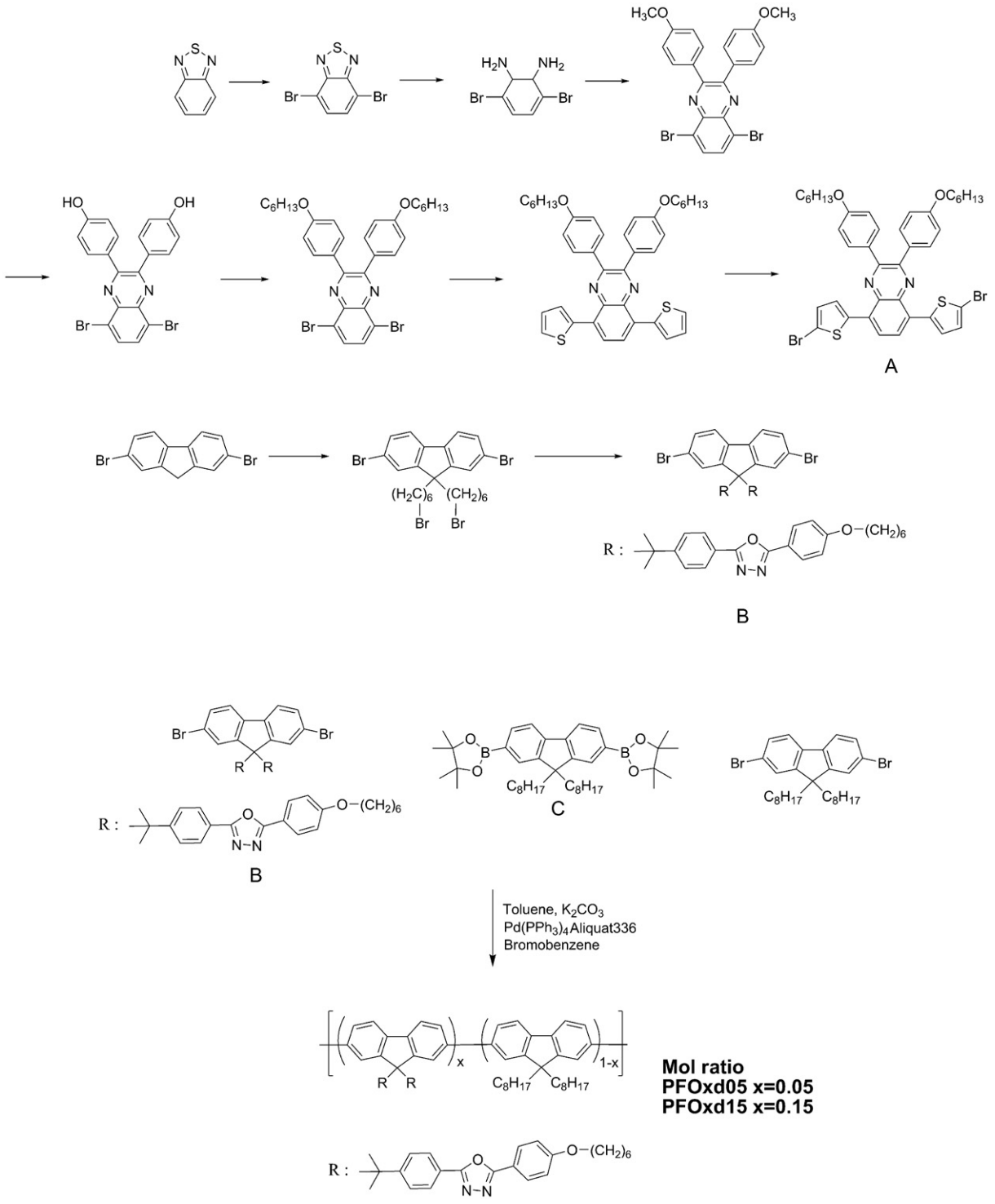

Scheme 1. Monomer synthesis and polymerization of PFOxd05, PFOxd15.

Table 2
Optical and electrochemical properties of polymers.

Polymer	Solution, λ_{max} (nm)		Film, λ_{max} (nm)		E_{HOMO} (eV)	E_{LUMO} (eV)
	Absorption	Emission	Absorption	Emission		
PF	389	418, 439	382	422, 441	5.78	2.83
PFOxd05	388	418, 440	382	424	5.82	2.87
PFOxd15	302, 388	418, 440	302, 382	424, 445	5.95	3.00
PFOxd15TQ03	302, 389	417, 439	301, 384	422, 445	5.95	3.00
PFOxd15TQ05	301, 388	417, 439	302, 384	424, 444	5.95	3.00
PFOxd15TQ10	302, 388	417, 439	302, 384	422, 445, 571	5.95	3.00
PFTQ10	385	416, 439	382	437, 460, 589	5.84	2.89

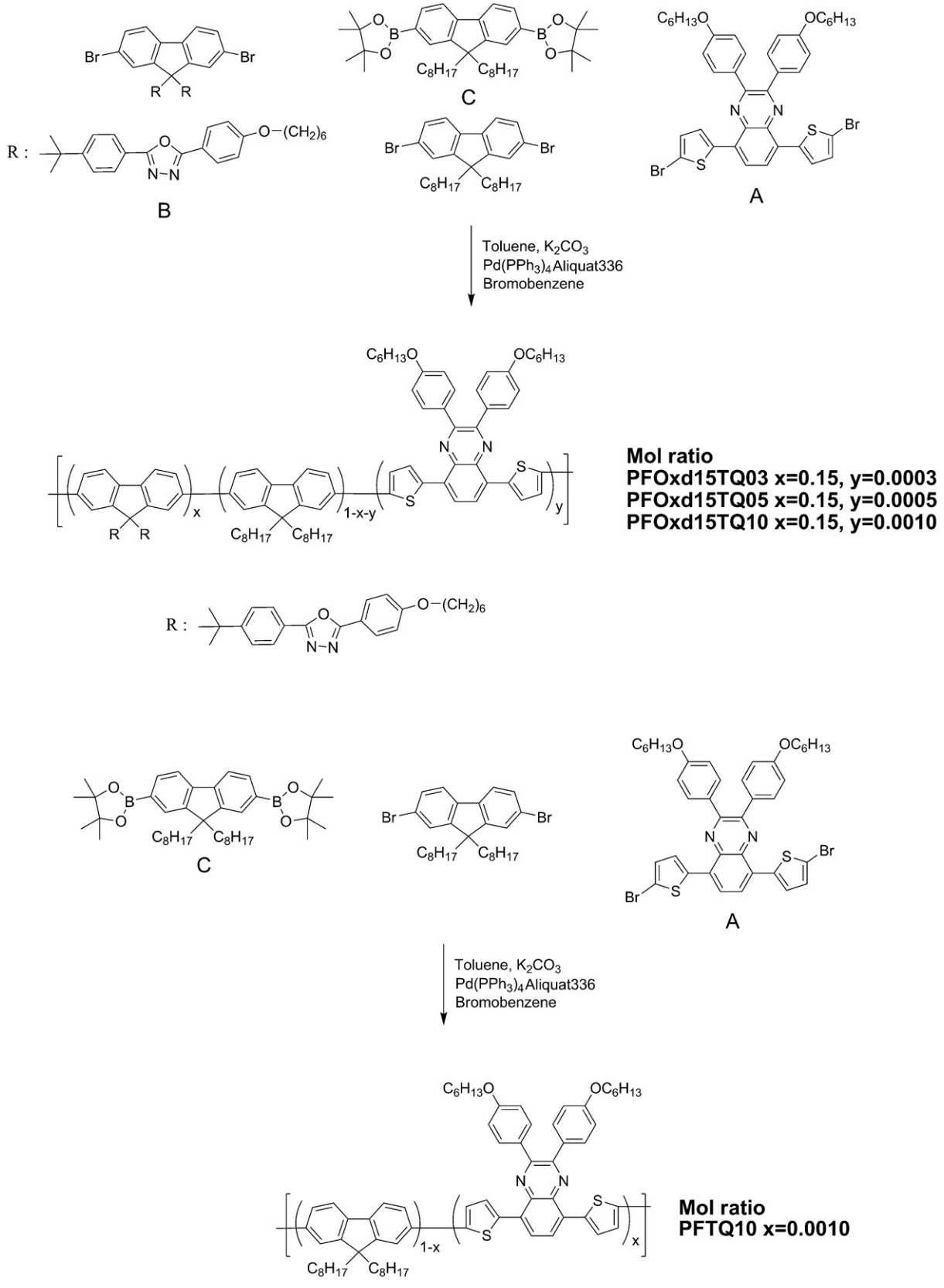

Scheme 2. Polymerization of PFOxd15TQ03, PFOxd15TQ05, PFOxd15TQ10, PFTQ10.

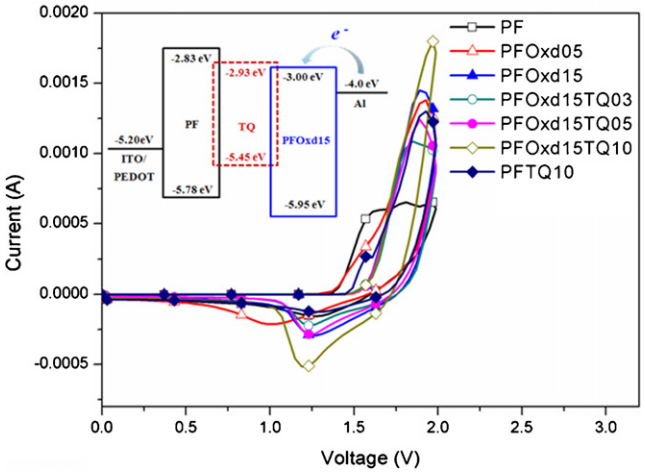

Fig. 2. Cyclic voltammograms of polymers and band diagram of PF, BT and POR.

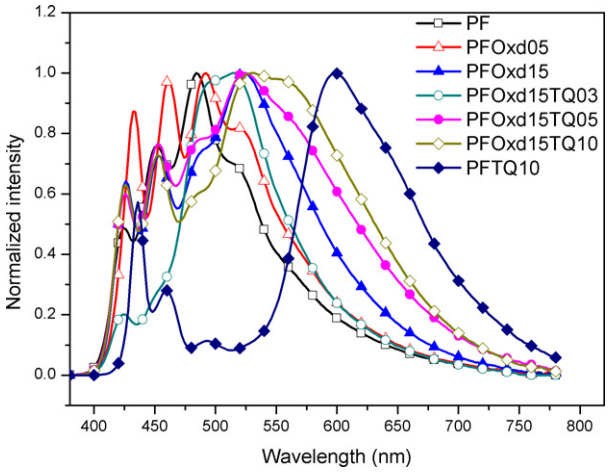

Fig. 3. EL luminescence spectra of polymers.

In contrast, the lowest unoccupied molecular orbital (LUMO) levels were estimated based on the difference between the HOMO level and the optical band gap calculated from UV–vis absorption onset value of polymer thin film. The HOMO and LUMO levels of the polymers and optical band gap are exhibited in Table 2.

The HOMO levels of PF, PFOxd05 and PFOxd15 were −5.78, −5.82 and −5.95 eV and the LUMO levels were −2.83, −2.87 and −3.00 eV, respectively. As the amount of oxadiazole derivative increased, the HOMO and LUMO levels decreased because of the strong electron withdrawing characteristics of the oxadiazole derivative. In terms of the HOMO and LUMO levels, PFOxd15TQ03, PFOxd15TQ05 and PFOxd15TQ10 were the same as PFOxd15, because the TQ dopant content was very small (0.1 mol% or less), having little effect on the polymer backbone [5]. The inset in Fig. 2 shows the energy band diagrams of PF, PFOxd15 and TQ derivative. As shown in these diagrams, the energy level of the TQ dopant exists between the HOMO and LUMO levels of PF. In contrast, the dopant TQ energy level is slightly higher than the LUMO level of PFOxd15. It was expected that charge trapping would effectively occur from PF to TQ compared to PFOxd15 [5,35]. In addition, because PFOxd15 (−3.00 eV) had lower LUMO level than that of PF (−2.83 eV) by 0.17 eV, more effective electron injection is enabled in PFOxd15.

3.3. Electroluminescence properties and current–voltage–luminance characteristics

Fig. 3 shows the electroluminescent spectra of the EL device. The brightness–voltage and efficiency–current density of the EL device are shown in Fig. 4(a) and (b), respectively, and their characteristics are summarized in Table 3. The device was fabricated with ITO/PEDOT:PSS/polymer/BaF_2/Ba/Al structure, as shown in the inset of Fig. 4(a), and the emission layer was fabricated to 70–80 nm thickness through spin-coating. As shown in Fig. 3, emissions increased at 524 nm in PFOxd05 and PFOxd15 compared to PF because of increased emission by oxadiazole [27]. In

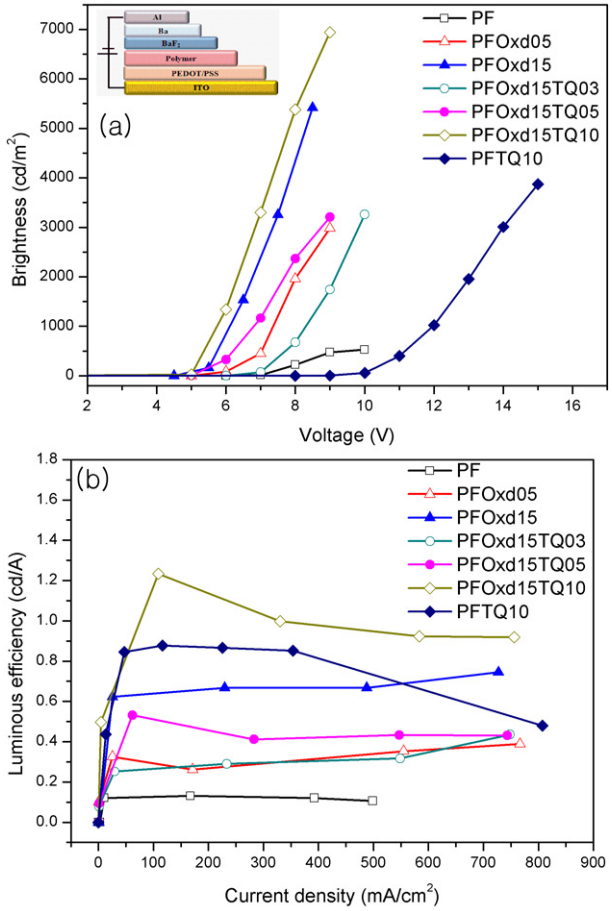

Fig. 4. (a) voltage–luminance (*V–L*), (b) current density–luminous efficiency (*J–LE*) curve.

Table 3
Summary of EL device performances of polymers.

Polymer	EL emission λ_{max} (nm)	Luminous efficiency (cd/A)	Power efficiency (lm/W)	Maximum brightness (cd/m²)	CIE coordinate (*x*, *y*)
PF	424, 452, 484	0.13	0.05	527	(0.21, 0.29)
PFOxd05	432, 462, 492	0.32	0.17	2978	(0.22, 0.31)
PFOxd15	426, 454, 524	0.74	0.35	5415	(0.27, 0.38)
PFOxd15TQ03	424, 516	0.43	0.13	3258	(0.25, 0.44)
PFOxd15TQ05	426, 452, 524	0.53	0.27	3205	(0.30, 0.38)
PFOxd15TQ10	426, 452, 532	1.23	0.64	6940	(0.33, 0.39)
PFTQ10	436, 460, 598	0.84	0.24	3872	(0.48, 0.34)

case of PFOxd15TQ03, PFOxd15TQ05 and PFOxd15TQ10, emissions broadened at 550–650 nm as the TQ derivative content increased, because of incomplete energy transfer from fluorene derivative to TQ derivative. Furthermore, as TQ derivative content increased, spectra intensity increased at 550–650 nm with similar pattern to the PL spectra. In case of PFTQ10, on the other hand, energy was mostly transferred from fluorene derivative to TQ derivative, and then, broad emission was detected around 598 nm. As a result, it has been confirmed that the oxadiazole derivative plays a role in suppressing the energy transfer from fluorene derivative to TQ derivative.

Overall, differences were found between the PL spectra and EL spectra. Unlike in the PL spectra, similar intensity was found in green and red emissions (λ_{max} = 524, 571 nm) in the blue emission (λ_{max} = 432 nm) of the EL spectra. It has been confirmed that the low energy level of TQ derivative worked as a charge trapping site. This kind of result is matched with the HOMO and LUMO levels of the dopant confirmed in electrochemical measurements [5,19]. As shown in Table 3, the CIE coordinates of PFOxd15TQ05 and PFOxd15TQ10 were (0.30, 0.38) and (0.33, 0.39), respectively, which are close to the pure white coordinates of (0.33, 0.33).

According to the Voltage–Luminescence (V–L) curve in Fig. 4(a), the turn-on voltage tended to decline from 7 to 5 V as the oxadiazole derivative content increased in PF, PFOxd05 and PFOxd15. The turn-on voltage of PFOxd15TQ10 and PFTQ10 were 5 V and 10 V, respectively. The turn-on voltage of PFOxd15TQ10 significantly decreased to 5 V, unlike that of PFTQ10, because effective electron injection was enabled by the oxadiazole derivative with superior electron withdrawing characteristics [30]. This kind of result is matched with the result that the PFOxd15 LUMO level (−3.00 eV) was lower than the PFTQ10 LUMO level (−2.89 eV) in CV measurements, as shown in Fig. 3.

The best EL performance was exhibited in PFOxd15TQ10, which was observed with 1.23 cd/A luminous efficiency, 0.64 lm/W power efficiency, 6940 cd/m^2 maximum brightness, and CIE coordinates of (0.33, 0.39). As shown in Fig. 4(b), as current density increased, the luminous efficiency stayed stable in PFOxd15TQ10. Stable luminous efficiency and the best performance occurred in PFOxd15TQ10 because of the well-balanced electron and hole injection in the oxadiazole-TQ derivative ratio and effective energy transfer and charge trapping between fluorene derivative and TQ derivative [5,35]. In terms of EL performance, that of PFTQ10 was relatively poorer than that of PFOxd15TQ10 because effective electron injection did not occur due to the high LUMO level. In addition, the TQ derivative worked as a charge trapping site along the polymer backbone and exhibited exciton quenching [19].

According to an analysis on the CIE coordinates (1931) (see Fig. S5) of all polymers, oxadiazole derivative content increased, and emission ranging from blue to light green in PF, PFOxd05 and PFOxd15 was shown. As confirmed above, green emissions (λ_{max} = 524 nm) increased as oxadiazole derivative content increased [30]. The CIE coordinates of PFOxd15TQ05 and PFOxd15TQ10 were (0.30, 0.38) and (0.33, 0.39), respectively, which is close to pure white (0.33, 0.33). In case of PFTQ10, in contrast, energy was mostly transferred from fluorene to the TQ derivative, and charge trapping occurred. As a result, light-red emissions were observed with CIE coordinates of (0.48, 0.34).

4. Conclusions

We successfully synthesized white-emitting polymers containing oxadiazole and TQ on a PF backbone. The synthesized PFOxd series polymers showed good solubility and thermal stability. In case of PL spectra, as TQ content increased, the 570 nm emission peak broadened, unlike in solution, because of increased intermolecular interaction among polymer main chains. The red-shift phenomenon which occurs on the film due to strong intermolecular interaction among polymers significantly declined in the PFOxd series polymers containing oxadiazole derivative. In an EL device, PFOxd15TQ10 had stable and superior performance, because the ratio of oxadiazole and TQ was well balanced between electron and hole injection in the device, and energy transfer was effectively processed between fluorene derivatives, oxadiazole, and TQ derivatives. The luminous efficiency, maximum brightness, and CIE coordinates of the device were 1.23 cd/A, 6940 cd/m^2, and (0.33, 0.39), close to white emission, respectively.

Acknowledgment

This work was supported by the Konkuk University.

Appendix A. Supplementary data

Supplementary data associated with this article can be found, in the online version, at http://dx.doi.org/10.1016/j.synthmet.2012.11.004.

References

[1] R.H. Friend, R.W. Gymer, A.B. Holmes, J.H. Burroughes, R.N. Marks, C. Taliani, D.D.C. Bradley, D.A. Dos Santos, J.L. Bredas, M. Logdlund, W.R. Salaneck, Nature 397 (1999) 121–128.
[2] C. Ulbricht, B. Beyer, C. Friebe, A. Winter, U.S. Schubert, Advanced Materials 21 (2009) 4418–4441.
[3] H.J. Song, J.Y. Lee, I.S. Song, D.K. Moon, J.R. Haw, Journal of Industrial and Engineering Chemistry 17 (2011) 352–357.
[4] M. Kijima, I. Kinoshita, T. Hattori, H. Shirakawa, Synthetic Metals 100 (1999) 61–69.
[5] H.J. Song, D.H. Kim, T.H. Lee, D.K. Moon, European Polymer Journal 48 (2012) 1485–1494.
[6] H. Wu, L. Ying, W. Yang, Y. Cao, Chemical Society Reviews 38 (2009) 3391–3400.
[7] A. Gadisa, W. Mammo, L.M. Andersson, S. Admassie, F. Zhang, L. Chen, M.R. Andersson, O. Inganäs, Advanced Functional Materials 23 (2007) 3836–3842.
[8] E. Wang, L. Hou, Z. Wang, S. Hellström, F. Zhang, O. Inganäs, M.R. Andersson, Advanced Materials 22 (2010) 5240–5244.
[9] J.Y. Lee, S.H. Kim, I.S. Song, D.K. Moon, Journal of Materials Chemistry 21 (2011) 16480–16487.
[10] J.Y. Lee, A.N. Aleshin, D.W. Kim, H.J. Lee, Y.S. Kim, G. Wegner, V. Enkelmann, S. Roth, Y.W. Park, Synthetic Metals 152 (2005) 169–172.
[11] I. Mcculloch, M. Heeney, C. Bailey, K. Genevicius, I. Macdonald, M. Shkunov, D. Sparrowe, S. Tierney, R. Wagner, W. Zhang, M.L. Chabinyc, R.J. Kline, M.D. Mcgehee, M.F. Toney, Nature Materials 5 (2006) 328–333.
[12] I. Osaka, M. Shimawaki, H. Mori, I. Doi, E. Miyazaki, T. Koganezawa, K. Takimiya, Journal of the American Chemical Society 134 (2012) 3498–3507.
[13] M. Goh, S. Matsushita, K. Akagi, Chemical Society Reviews 39 (2010) 2466–2476.
[14] M.M. Alam, S.A. Jenekhe, Chemistry of Materials 14 (2002) 4775–4780.
[15] J.H. Burroughes, D.D.C. Bradley, A.R. Brown, R.N. Marks, K. Mackay, R.H. Friend, P.L. Burns, A.B. Holmes, Nature 347 (1990) 539–541.
[16] Q. Pei, Y. Yang, Journal of the American Chemical Society 118 (1996) 7416–7417.
[17] Z. Tan, R. Tang, E. Zhou, Y. He, C. Yang, F. Xi, Y. Li, Applied Polymer Science 107 (2008) 514–521.
[18] X.Y. Deng, W.M. Lau, K.Y. Wong, K.H. Low, H.F. Chow, Applied Physics Letters 84 (2004) 3522.
[19] M.J. Park, J.H. Lee, I.H. Jung, J.H. Park, D.H. Hwang, H.K. Shim, Macromolecules 41 (2008) 9643–9649.
[20] Q. Hou, Y. Xu, W. Yang, M. Yuan, J. Peng, Y. Cao, Journal of Materials Chemistry 12 (2002) 2887–2892.
[21] M. Sun, Q. Niu, B. Du, J. Peng, W. Yang, Y. Cao, Macromolecular Chemistry and Physics 208 (2007) 988–993.
[22] E. Xu, H. Zhong, H. Lai, D. Zeng, J. Zhang, W. Zhu, Q. Fang, Macromolecular Chemistry and Physics 211 (2010) 651–656.
[23] A. Tsami, X.H. Yang, F. Galbrecht, T. Farrell, H. Li, S. Adamczyk, R. Heiderhoff, L.J. Balk, D. Neher, E. Holder, Journal of Polymer Science Part A: Polymer Chemistry 45 (2007) 4773–4785.
[24] Y.K. Lee, Y.M. Nam, W.H. Jo, Journal of Materials Chemistry 21 (2011) 8583–8590.
[25] N. Blouin, A. Michaud, D. Gendron, S. Wakim, E. Blair, R. Neagu-Plesu, M. Bellete^te, G. Durocher, Y. Tao, M. Leclerc, Journal of the American Chemical Society 130 (2008) 732–742.
[26] M.C. Yuan, P.I. Shih, C.H. Chien, C.F. Shu, Journal of Polymer Science Part A: Polymer Chemistry 45 (2007) 2925–2937.
[27] H. Tan, J. Yu, Y. Wang, J. Li, J. Cui, J. Luo, D. Shi, K. Chen, Y. Liu, K. Nie, W. Zhu, Journal of Polymer Science Part A: Polymer Chemistry 50 (2012) 149–155.

[28] J. Deng, Y. Liu, Y. Wang, H. Tan, Z. Zhang, G. Lei, J. Yu, M. Zhu, W. Zhu, Y. Cao, European Polymer Journal 47 (2011) 1836–1841.
[29] C.W. Wu, C.M. Tsai, H.C. Lin, Macromolecules 39 (2006) 4298–4305.
[30] Y.E. Jin, J.Y. Kim, S.H. Park, J.W. Kim, S.E. Lee, K.H. Lee, H.S. Suh, Polymer 46 (2005) 12158–12165.
[31] B.Y. Hsieh, Y. Chen, Journal of Polymer Science Part A: Polymer Chemistry 47 (2009) 833–844.
[32] H.J. Song, S.M. Lee, J.Y. Lee, B.H. Choi, D.K. Moon, Synthetic Metals 161 (2011) 2451–2459.
[33] J. Xu, Y. Zhang, J. Hou, Z. Wei, S. Pu, J. Zhao, Y. Du, European Polymer Journal 42 (2006) 1154–1163.
[34] J. Ding, M. Day, G. Robertson, J. Roove, Macromolecules 35 (2002) 3474–3483.
[35] Q. Chen, N. Liu, L. Ying, W. Yang, H. Wu, W. Xu, Y. Cao, Polymer 50 (2009) 1430–1437.